Biomedicine & Pharmacotherapy 172 (2024) 116201

Contents lists available at ScienceDirect

Biomedicine & Pharmacotherapy

journal homepage: www.elsevier.com/locate/biopha

Canine glioblastoma-derived extracellular vesicles as precise carriers for glioblastoma imaging: Targeting across the blood-brain barrier

Alessandro Villa [a], Zemira De Mitri [a], Simona Vincenti [b], Elisabetta Crippa [a], Laura Castiglioni [c], Paolo Gelosa [c], Monica Rebecchi [a], Delfina Tosi [a], Electra Brunialti [a], Anna Oevermann [d], Monica Falleni [a], Luigi Sironi [c], Lorenzo Bello [e], Vincenzo Mazzaferro [e,f], Paolo Ciana [a,*]

[a] Department of Health Sciences, University of Milan, via A. di Rudinì, 8, 20142, Milano, Italy
[b] Department of Clinical Veterinary Medicine, Vetsuisse Faculty, University of Bern, Länggassstrasse 124, 3001 Bern, Switzerland
[c] Department of Pharmaceutical Sciences, University of Milan, via Balzaretti, 20133 Milano, Italy
[d] Division of Neurological Sciences, Department of Clinical Research and Veterinary Public Health, Vetsuisse Faculty, University of Bern, Länggassstrasse 124, 3001 Bern, Switzerland
[e] Department of Oncology and Hemato-Oncology, Università Degli Studi di Milano, Via Festa del Perdono 7, 20122 Milano, Italy
[f] HPB Surgery and Liver Transplantation, Fondazione IRCCS Istituto Nazionale Tumori (INT), Via Giacomo Venezian, 1, 20133 Milano, Italy

ARTICLE INFO

Keywords:
Drug delivery
MRI
Orthotopic glioblastoma
Canine EVs
Murine models

ABSTRACT

The treatment of glioblastoma (GBM) faces significant challenges due to the difficulty of delivering drugs through the blood-brain barrier (BBB). Extracellular vesicles (EVs) have emerged as potential carriers for targeted drug delivery to brain tumors. However, their use and distribution in the presence of an intact BBB and their ability to target GBM tissue are still under investigation. This study explored the use of EVs for GBM targeting across the BBB. Canine plasma EVs from healthy dogs and dogs with glioma were isolated, characterized, and loaded with diagnostic agents. Biodistribution studies were conducted in healthy murine models and a novel intranasal model that preserved BBB integrity while initiating early-stage GBM growth. This model assessed EVs' potential for delivering the contrast agent gadoteric acid to intracranial tumors. Imaging techniques, such as bioluminescence and MRI, confirmed EVs' targeting and delivery capabilities thus revealing a selective accumulation of canine glioma-derived EVs in brain tissue under physiological conditions. In the model of brain tumor, MRI experiments demonstrated the ability of EVs to accumulate gadoteric acid within GBM to enhance contrast of the tumoral mass, even when BBB integrity is maintained. This study underscores the potential of EVs derived from glioma for the targeted delivery of drugs to glioblastoma. EVs from dogs with glioma showed capacity to traverse the BBB and selectively accumulate within the brain tumor. Overall, this research represents a foundation for the application of autologous EVs to precision glioblastoma treatment, addressing the challenge of BBB penetration and targeting specificity in brain cancer therapy.

1. Introduction

The identification of diagnostic tools for the early detection of neoplastic growth is a significant challenge in the field of oncology. This challenge becomes even more critical when considering the diagnosis and excision of glioblastoma, which stands as the most prevalent and aggressive type of primary malignant brain tumor [1]. Glioblastomas are characterized by their rapid growth, invasive behavior, and high propensity for recurrence. Their treatment complexity stems from their capability to infiltrate the surrounding brain tissue, rendering complete surgical extraction a difficult task [1]. Because of the complexity of glioblastomas and their aggressive behavior, research efforts aim at developing more effective treatment strategies; in particular, early diagnosis is crucial for improving treatment outcomes, but due to the complexities of the disease and the lack of specific early symptoms, it remains a challenging effort [2]. Indeed, glioblastomas often grow rapidly and may not cause noticeable symptoms until they have reached a significant size or have already invaded surrounding brain tissue. Additionally, early detection using standard brain imaging techniques is difficult, because early-stage glioblastomas might not show significant

* Corresponding author.
E-mail address: paolo.ciana@unimi.it (P. Ciana).

https://doi.org/10.1016/j.biopha.2024.116201
Received 11 October 2023; Received in revised form 11 January 2024; Accepted 22 January 2024
Available online 1 February 2024

contrast enhancement, making them harder to distinguish from surrounding brain tissue [2]. Indeed, current diagnostic methodologies, including magnetic resonance imaging (MRI) and computed tomography (CT), necessitate the intravenous administration of contrast agents, such as paramagnetic molecules for MRI or iodine-containing compounds for CT [3]. These diagnostic agents demonstrate an affinity for tumor regions due to the prevailing enhanced permeability and retention (EPR) effect, characteristic of tumor-associated endothelial permeability, which leads to the passive accumulation of contrast agents – but also of therapeutic drugs and other molecules - in the tumor microenvironment [4]. However, in gliomas the extravasation of contrast agents into the tumor microenvironment is attained only when the BBB shows augmented permeability, a phenomenon induced when the mass of glioblastoma already reached a critical size [5]. For this reason, conventional contrast agents are impeded from traversing the BBB, restricting their access to the neoplastic cerebral mass primarily during advanced tumor stages: in such cases, these imaging modalities provide valuable information about the location, size, characteristics, and extent of brain tumors, aiding in their diagnosis, treatment planning, and monitoring [3]. For this reason, there is increasing interest in the development of novel diagnostic techniques based on MRI and CT, with the aim of facilitating the identification of the tumor boundaries also during surgical interventions, thereby enabling a complete and precise tumor excision [6]. In this context, a method for precisely delivering diagnostic molecules, as well as potentially therapeutic substances, across the BBB to glioma tumor cells is certainly needed: if available, such a technology would enable the detection of neoplastic cells even at the initial stages when the BBB remains functionally intact, consequently augmenting the efficacy of targeted surgical modalities in achieving comprehensive and precise tumor eradication, while concurrently mitigating the risk of recurrence. In response to this need, the potential role of extracellular vesicles (EVs) emerges as a potential route for tumor-targeted therapeutic and diagnostic applications. Indeed, EVs are membrane vesicles present in biological fluids, which physiological function is to precisely transport coding or noncoding RNA molecules, proteins, lipids and small molecules to the target cells [7]. This precise delivery capability drew the attention of pharmacologists, who quickly found that drugs could be encapsulated in these natural nanoparticles for the delivery to specific cells [8]. More interestingly, it has been discovered that cancer cells produce specific EVs able to convey the cargo contained inside their phospholipid membrane to the neoplastic tissue through a very precise homing mechanism that is extensively conserved across species, as described in various scientific studies [9–11]. This has been proven to be true not only for tumoral cell lines, but also for the tumors developed in the oncological patients: indeed, plasma of oncology patients is enriched in EVs that, unlike those isolated from healthy persons, have been shown to selectively target the originating tumor [11]. Recently, some evidence has suggested that EVs can cross the BBB [12,13], thus supporting the use of these nanoparticles as a possible option for delivering drugs to the brain. Based on these assumptions, we hypothesized that suitable EVs loaded with contrast agents would allow the diagnostic molecule to be transported even through an intact BBB, thereby increasing the contrast of the tumor in medical images and, eventually, allowing the precise localization of malignant tissue for early diagnosis. To test our hypothesis, we explored the possibility of isolating EVs from the plasma of dogs with glioma (CG-EVs), and to load them with diagnostic molecules, with the final aim of evaluating if EVs released by glioma are able to cross the BBB and specifically recognize glioblastoma. To this purpose we loaded CG-EVs with a fluorescent dye (indocyanine green) and with gadoteric acid (Gd-DOTA), a contrast agent for MRI, to investigate through molecular imaging techniques the homing of these EVs in murine models of glioblastoma.

2. Materials and methods

2.1. Cell cultures

The cell line used is the murine glioma cell line CT2A, purchased from Merck. The cell line was generated from a malignant astrocytoma obtained by implanting the carcinogen 20-methylcholanthrene into the brain of C57L/6 J mice. The cell culture medium is DMEM (Gibco) supplemented with 10% FBS (Merck). Neurospheres were obtained from the CT2A murine glioma cell line cultured in DMEM F12, 2% B27 supplement (Gibco), 20 ng/mL FGF (Gibco), and 20 ng/mL EGF (Sigma Aldrich) for 7–8 days.

2.2. EV Isolation from blood

Venous blood (15 mL) was collected from three dogs which spontaneously developed brain tumors and had a radiological diagnosis of glioma during preoperative analyses and three healthy dogs after approval of the Ethics Committee of the Small Animal Clinic of the University of Bern (Aut n. BE134/2020). Human EV sample was derived from a venous blood (20 mL) withdraw from a colorectal cancer patient after approval by the Ethics Committee of the National Cancer Institute of Milan (Aut. INT 244/20), and informed consent was obtained for experimentation. Blood was collected in EDTA-conditioned vials and immediately centrifuged at 1750g for 10 min at room temperature to remove blood cells and prevent platelet activation and the release of platelet-derived EVs. Supernatants were transferred to new tubes (the bottom 10% of supernatant above the blood cells was discarded), and samples were centrifuged again at 3000g for 10 min at room temperature. Supernatants were collected and processed by ultracentrifugation for 2 h at 100,000g at 4 ∘C in an Optima L-80 XP ultracentrifuge (Beckman Coulter, Indianapolis, IN, USA) with an SW32Ti rotor (Beckman Coulter). Supernatants were aspirated and the EV-containing pellets were resuspended in 150 μL phosphate-buffered saline (DPBS, EMD Millipore, Burlington, MA, USA) and stored at − 80 ∘C until use.

2.3. Size distribution determination by nanoparticle tracking analysis (NTA)

The size distribution and concentration of EV were analyzed by Nanoparticle Tracking Analysis (NTA) using a Nanosight model NS300 (Malvern Panalytical Ltd, Malvern, UK) NTA with a blue (404 nm, 70 mV) laser and sCMOS camera. NTA was performed for each sample by recording three 60 s videos, which were subsequently analyzed using NTA software 3.0 (Nanosight). The detection threshold was set to level 5 and the camera to level 10.

2.4. Cryo trasmission-electron microscopy (TEM)

Cryo-TEM images (150 fields) were acquired with a JEOL electron microscope equipped with an FEI Falcon 3EC direct electron detector and Volta Phase-plate. Prior to Cryo-EV imaging, the samples were vitrified on a FEI Vitrobot IV system and processed as previously reported.

2.5. Immunoblotting

For immunoblotting, EVs were isolated from blood of dogs with glioma according to the protocol described above. After the ultracentrifugation step, the supernatants were removed and the EV-containing pellets were resuspended in a proper volume of 1X RIPA buffer (150 mM NaCl; 1% NP-40; 0.5% sodium deoxycholate; 0.1% SDS; 50 mM Tris-HCl, pH 8.0) supplemented with protease inhibitor cocktail (Roche, Penzberg, Germany). EV protein concentrations were quantified using a Bradford assay kit (ThermoFischer Scientific, Waltham, MA, USA). Twenty micrograms of EV protein lysates were separated to 4–10% SDS-

PAGE using beta-mercaptoethanol as the reducing agent and transferred to nitrocellulose membranes (Amersham Biosciences, Amersham, UK). The membranes were then blocked in 5% nonfat dry milk in TBS-T (0.2% Tween-20) at RT and incubated overnight with the primary antibody against exosomal TSG101 (4A10, 1:500, Abcam, Cam- bridge, MA, USA). After that, the membranes were incubated for 1 h at RT with the secondary antibody. Immunoreactive bands were visualized with chemiluminescence using the ECL Western Blotting Analysis System according to the manufacturer's instructions (Amersham Biosciences, Amersham, UK).

2.6. EV loading with gadolinium and Indocyanine Green (ICG)

Gadolinium (Gd) is a silvery-white, malleable, and ductile rare-earth metal. Gd has paramagnetic properties and, therefore, solutions of organic Gd complexes and Gd compounds are commonly used intravenously for magnetic resonance imaging (MRI) as contrast agents able to permeate into the EV membranes. For this reason, passive diffusion was used to load EVs with gadolinium. Incubation with gadolinium was carried out by adding 10^8 CG-EVs suspended in 50 μL of Dulbecco's phosphate buffered saline (DPBS, EMD Millipore, Burlington, Massachusetts, United States) to 950 μL of Gd-DOTA (Acidum Gadotericum Clariscan Injection 0.5 mmol/mL, GE Healthcare, Milano, Italia). The mix was incubated for 16 h at 4 °C. Then, samples were brought to a volume of 25 mL with DPBS and ultracentrifuged at 100,000g for 90 min at RT (Himac ultracentrifuge CP100NX with rotor P50AT2, Eppendorf Himac Technologies Co., Takeda, Japan). After ultracentrifugation, the supernatant was eliminated and the EV-containing pellets were resuspended in 150 μL DPBS. ICG was loaded into CG-EVs as previously described (Villa et al., 2021). Briefly, 10^8 CG-EVs suspended in 50 μL DPBS were added to 150 μL of a water solution of 5 mg/mL ICG (Sigma) and incubated for 16 h at 4 °C. Then, samples were ultracentrifuged at 100,000g for 90 min. After supernatant removal, pellets were resuspended in 150 μL of DPBS.

2.7. Mice

All animal experiments were approved by the Italian Ministry of Research and University (permission number: 214/2020) and regulated by a departmental panel of experts. C57BL/6NCrl (Charles River, MGI: 2683688) mice were maintained at the animal facility of the University of Milan under standard conditions according to institutional guidelines. These mice are NFkB-luc transgenic, in which the expression of luciferase is controlled by the NFkB transcription factor, which is an important regulator of the pro-inflammatory response. After an acclimatization period of 14 days, murine syngeneic grafts were established by subcutaneous injections of 4×10^6 CT-2A cells into the neck of 12-week-old male C57BL/6 mice. The CT-2A cell line, purchased from Merck, is derived from a sub-cutaneous, non-metastatic murine glioma (astrocytoma) formed via implantation of the carcinogen 20-methylcholanthrene in the cerebrum of a C57BL/6 J mouse. In order to test the homing capability of the EVs to the tumor in the brain, other mice were injected intranasally with 4×10^6 CT2A cells and EVs injections were performed 1 month after cells injection. The health status of the mice in the experimentation was monitored daily, and as soon as signs of pain or distress were evident, the mice were euthanized. EV injections in subcutaneous glioma model were performed when the tumor size reached a diameter of ~10 mm. For the homing tests, mice with tumors were intravenous injected with 2–4 $\times$ 10^9 EVs/kg, through a retro-orbital injection.

2.8. In vivo bioluminescence imaging

To evaluate the brain tumor growth in NFkB mice, inflammation associated with tumor development was analyzed through *in vivo* bioluminescence imaging. A total amount of 80 μL of luciferin was injected with intraperitoneal administration and after 5 min, the bioluminescent signal was detected using an *in vivo* imaging system (IVIS CAMERA, Perkin Elmer). The 3D localization of the signal was obtained using Living Image software.

2.9. In vivo and ex vivo fluorescence imaging

In vivo and *ex vivo* fluorescence imaging was carried out 24 h after EVs treatment using a IVIS camera (PerkinElmer), equipped with filters for near-infrared signal detection, following the manufacturer's instructions. Mice were anaesthetized using isoflurane (Isoflurane-V et; Merial, Lyon, France) and kept under anesthesia during imaging sessions. For *ex vivo* imaging, mice were sacrificed by cervical dislocation. Immediately after death, fluorescence signal from selected organs was analysed.

2.10. MRI

To investigate the presence or absence of Gd-DOTA in murine glioma models, we carried out a magnetic resonance imaging analysis using 4.7 T, vertical super-wide bore magnet of a Bruker Avance II spectrometer with microimaging accessory. Mice were fixed on the holder and placed into the 6.4 cm diameter birdcage coil. A 3-orthogonal-plane, gradient echo scout acted as a geometric reference for locating the olfactory bulb. T1 weighted acquisition parameters were: repetition time (TR) = 436 ms, effective echo time (TE) = 10 ms, number of averages (NA) = 12, matrix resolution = 128 × 128, FOV field of view (FOV) = 4 cm x 3 cm, in-plane resolution = 312 μm^2/pixel^2 x 234 μm^2/pixel^2 slice thickness = 1 mm, interslice distance = 1 mm and number of contiguous slices = 18. Twelve signal averages were recorded for a total scan time of 11 min and 9 s. Contrast agent was identified as areas of high signal intensity.

To quantify Gd-DOTA loading efficiency within canine EVs, MRI T1 weighted analysis was performed on Gd-DOTA loaded CG-EVs, Gd-DOTA standard curve (0.5 mM to 5 nM) as reference and empty CG-EVs. T1 weighted acquisition parameters were: repetition time (TR) = 387 ms, effective echo time (TE) = 10 ms, number of averages (NA) = 12, matrix resolution = 128 × 128, field of view (FOV) = 4 cm x 3 cm, in-plane resolution = 312 μm^2/pixel^2 x 234 μm^2/pixel^2, resolution = 0.312 × 0.234, slice thickness = 2 mm, interslice distance = 4 mm and number of contiguous slices = 2. Twelve signal averages were recorded for a total scan time of 9 min and 55 s. The Gd-DOTA loading efficiency was measured using three different lots of Acidum Gadotericum Clariscan (lot:15729411, lot:15986847, lot: 06GS667A), to evaluate batch effects in loading efficiency. Each used lot led to similar loading efficiency.

2.11. Histological examination

Mice brains were fixed in 10% buffered formalin and frontal sections in correspondence of the bioluminescent areas were performed. Serial 5-μm sections from paraffin-embedded material were cut and stained with hematoxylin and eosin until detection of neoplastic infiltration.

2.12. Statistical analysis

Data were presented as the mean ± standard error. The statistical analysis was performed using PRISM (GraphPad, Version 9.1). T-test was used to compare the differences between two groups. $P < 0.05$ was considered to indicate a statistically significant difference.

3. Results

3.1. Characterization of plasma EVs from healthy dogs and dogs with glioma

EVs were isolated from whole blood samples (15 mL each) derived

from three dogs with glioma and two healthy dogs. To ensure adherence to established guidelines, the characterization of CG-EVs and EVs from healthy donors was conducted following the principles outlined in the "Minimal Information for Studies of Extracellular Vesicles (MISEV2018)" articles [14]. The dimension profile obtained with nanotracking analysis underscored that EVs from dogs with glioma were generally bigger than those obtained from healthy dogs, thus suggesting the existence of a specific EV population circulating in the blood of the dogs with glioma (Table 1).

As depicted in Fig. 1, the EVs displayed a size distribution ranging from 100 to 400 nm (Fig. 1A). Additionally, the presence of the distinctive biomarker TSG101 was identified in the EVs isolated (Fig. 1B and Supplementary Figure 1A), a finding that suggests the harvested fraction was enriched in exosomes. A confirmation of form, size, and structural integrity was obtained through Cryo-TEM imaging (Fig. 1C). Interestingly, while data on size and integrity show a congruence with the dimensional profile previously observed for EVs isolated from human donors [11], the counts indicate that dogs carry a greater number of circulating vesicles than humans. The evaluation of EV cargo loading efficiency was undertaken by subjecting the canine vesicles to passive incubation with Indocyanine Green (ICG). Post-incubation, a thorough washing process was implemented, and the fluorescence emitted by 10E08 canine EVs was compared to that released from the same number of EVs of human origin, which were concurrently incubated with ICG using the same methodology (see Supplementary Table 1). Notably, the overall fluorescence exhibited uniformity between the samples, signifying that the efficiency of ICG loading into EVs paralleled that previously ascertained for human EVs, which has been previously established as 150 nmol ICG per 10E08 particles via LC-MS [11]. Subsequently, the passive incubation approach was similarly applied to canine EVs for the purpose of Gd-DOTA loading. Quantification of Gd-DOTA loading efficiency within canine EVs was carried out through MRI analysis, where the T1-weighted MRI signal intensity was measured. This measurement was subsequently correlated with a standard curve containing varying concentrations (0.5 mM to 5 nM) of Gd-DOTA (Fig. 1E). In conclusion, the passive incubation methodology exhibited efficacy in loading canine EVs with Gd-DOTA, with a yield of 161 ± 24 nmol Gd-DOTA loaded in 10E08 EVs, as assessed through MRI analyses of EVs loaded with three different batches of Gd-DOTA, each of which led to a similar loading efficiency.

3.2. Exploring canine EVs for biodistribution in murine models

To our knowledge, this study represents the first investigation into the utilization of canine EVs in murine models. Therefore, in our initial experiment we started by comparing the kinetics of EV biodistribution in healthy mice. This approach aimed to establish the diffusion patterns of canine vesicles under physiological conditions. To achieve this, we loaded EVs obtained from both healthy dogs and dogs with glioma with ICG using the passive incubation protocol established by our laboratory.

Table 1
"Size distribution profile of canine EVs, acquired through NTA.".

ID	Dog w/ glioma 1	Dog w/ glioma 2	Dog w/ glioma 3	Healthy Dog 1	Healthy Dog 2
MEAN	190,7	190	190,7	143,2	142,3
MODE	149,3	129,5	141,4	88,7	84,3
SD	82,7	83,2	74,5	81,7	59
D10	108,3	111,7	124,4	80,9	82,4
D50	171,9	164,9	169,8	114,2	126,2
D90	296,4	315,8	294,5	255,1	233,1
EV/ mL	2,96E+ 10	2,72E+ 10	4,70E+ 10	7,10E+ 10	3,94E+ 10

SD: Standard deviation. D10: diameter (nm) of the particles that is the 10th percentile. D50: diameter (nm) of the particles that is the 50th percentile. D90: diameter (nm) of the particles that is the 90th percentile.

Subsequently, fluorescently labeled EVs were intravenously administered through a retro-orbital injection to two distinct groups of mice: the experimental group receiving CG-EVs (N = 3) and the control group receiving EVs isolated from healthy donors (N = 3). The biodistribution process was monitored through real-time fluorescence *in vivo* imaging at various time intervals: 0.5 h, 3 h, 6 h, and 24 h post-injection (Fig. 2). At this last time-point, a time-span sufficient for the complete wash-out of free ICG which has a biological half-life of 70–90 min, the animals were sacrificed and the biodistribution was evaluated also by *ex vivo* imaging (Fig. 2B-G).

Early time points (0.5 to 6 h) failed to reveal distinguishable biodistribution patterns between EVs derived from dogs with glioma and healthy dogs, likely reflecting a widespread distribution in the bloodstream throughout the body at the first timepoint, followed by a more localized distribution in the liver and GI anatomic areas, likely reflecting the excretion phases which for EVs usually occur via hepatobiliary pathways, (Fig. 2A). At the 24-hour mark, the *in vivo* imaging exhibited no discernible fluorescent signals in either group (Figs. 2B, E), thus suggesting that after this time frame, in the absence of a tumor, the fluorescent vesicles were unable to migrate and accumulate into the target tissue and were completely eliminated from the organism. Actually, *ex vivo* imaging performed on organs excised at 24 h, disclosed that EVs derived from dogs with glioma display a different accumulation pattern compared to that observed in vesicles derived from healthy canine donors. Specifically, the *ex vivo* imaging (Figs. 2C, F) revealed a notable fluorescence accumulation only within the brain region of the three animals exposed to CG-EVs (Fig. 2D), whereas such fluorescence localization in the brain was absent in mice subjected to EVs from healthy donors (Fig. 2D). This difference in the biodistribution suggests that, in the absence of tumors, canine glioma - derived vesicles are capable of crossing the BBB in healthy mice, with a propensity for accumulation within the brain tissue. Notably, the skull does not allow the fluorescent signal from the brain to be detected by the imaging device, which instead become measurable *ex vivo*, when the brain is directly exposed to the CCD-camera.

3.3. Evaluation of CG-EVs as transporters for targeted glioblastoma imaging

Having established the capability of CG-EVs to traverse the BBB, we proceeded to assess the homing potential of ICG-loaded CG-EVs in a straightforward tumor model that is routinely employed in our laboratory for evaluating the tumor tropism of ICG-loaded EVs. To outline the experimental design, C57BL/6 wild-type mice were subcutaneously implanted with a syngeneic cancer cell line - specifically, the murine glioma cell line CT2A. Through careful optimization of culturing conditions based on previously published protocols [15], we managed to generate neurospheres from CT2A cells. These neurospheres, characterized by being three-dimensional aggregates of glioma stem cells (GSCs), were demonstrated to effectively promote tumor growth and invasion [15]. Subsequently, we harvested and dissociated these neurospheres into a single-cell suspension, which we then injected subcutaneously into the neck area of six C57BL/6 wild-type mice at a concentration of 10E6 cells.

Over the subsequent seven-day period, as the subcutaneous tumors reached a size of approximately 6–8 mm^3, two groups of three mice each were intravenously injected through a retro-orbital injection with 5E08 ICG-loaded CG-EVs (N = 3) or an equivalent quantity of ICG-loaded EVs sourced from healthy donors, serving as controls (N = 3). Following a 24-hour interval, both *in vivo* and *ex vivo* fluorescence imaging were performed to evaluate the EV-mediated accumulation of ICG within the tumor tissue (Figs. 3A, B). Only mice treated with CG-EVs exhibited a robust fluorescent signal exclusively within the region of the subcutaneous tumor, as confirmed by the quantitative analysis of fluorescence in the excised organs (Fig. 3C). In this case the fluorescent signal is directly exposed to the CCD-camera detection, thus the light emission is

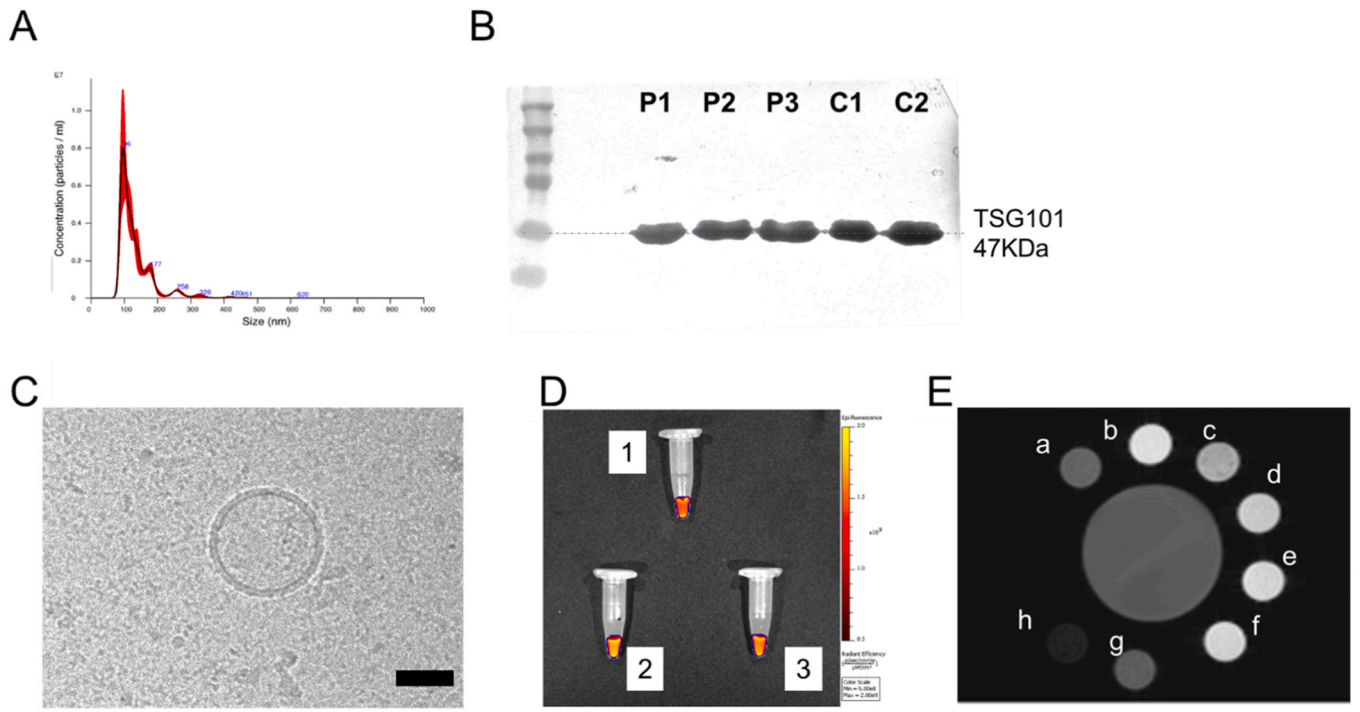

Fig. 1. Characterization of EVs from canine patients. The CG-EVs displayed size distribution, shape, EV-specific marker expression and cargo loading efficiency comparable with the patient-derived EVs used for the previous experiments. (A) Representative NTA analysis of particle size distribution of CG-EVs. The red line represents the standard error of the mean. Details on the size distribution and concentration are given in Table 1. (B) Immunoblot analysis of the Tumor Susceptibility Gene-101 (TSG101) expression in plasma-derived EVs from dogs with glioma (P1, P2, P3) or healthy controls (C1, C2). Loading control is reported in Supplementary Figure 1A. (C) Representative EV morphology and size obtained by acquiring 150 fields using cryo transmission electron microscopy, scale bar: 100 nm. Additional pictures are reported in Supplementary Figure 1B. D) Fluorescence analysis of samples of human EVs (1, top), CG-EVs (2, left) and healthy dog EVs (3, right). The representative picture shows the comparison of the fluorescence released by 10E8 ICG-loaded EVs per each sample, as acquired with a IVIS SpectrumCT imaging system. The intensity of the fluorescence signal (showing an average radiance of 1.4E09 in all the samples) is represented with pseudocolors: yellow: high photon emission (2E09 Radiant Efficiency), bright red: medium photon emission, and dark red: low photon emission (5E08 Radiant Efficiency). (E) Representative MRI scan of the setting used for the quantification of Gd-DOTA loading efficiency within canine EVs, showing the T1-weighted MRI signal intensity for standard samples and CG-EVs. a:Gd-DOTA loaded CG-EVs, b:Gd-DOTA 0.5 M, c-g:Gd-DOTA standard curve (0.5 mM to 5 nM), h: empty CG-EVs.

not shielded by the bone as instead is the case of the brain signal (Figs. 2A and C). In contrast, no discernible specific fluorescent signal was identified within the tumor in mice injected with EVs from healthy donors (Supplementary Figure 2). These results underscore that CG-EVs indeed facilitate the accumulation and stabilization of ICG, even in the context of glioblastoma. Remarkably, no fluorescent signal released from the brain was detected. This intriguing outcome suggests that in the presence of a peripheral tumor, CG-EVs show a preference for migration towards the tumor site, while in physiological settings devoid of tumoral cells, CG-EVs exhibit an inherent tendency to accumulate within the brain (Fig. 2C).

Once defined the tumor tropism of the CG-EVs, the subsequent investigation focused on determining whether Gd-DOTA-loaded CG-EVs maintained the ability to accumulate the contrast agent to the CT2A glioblastoma. To this end, we used a group of six mice bearing the same subcutaneous glioblastoma model described above. These mice were intravenously administered through retro-orbital injection either CG-EVs (N = 3) or EVs derived from healthy donors (N = 3), both loaded with Gd-DOTA. After a 24-hour interval, the animals were subjected to MRI analysis to assess the accumulation of the contrast agent within the tumor. Once more, the imaging analysis revealed a distinct hyperintense signal (Fig. 3F) localized precisely within the tumor site (Figs. 3D, E), originating from the accumulated contrast agent transported by CG-EVs. Indeed, this hyperintense signal was notably absent in the group that received EVs sourced from healthy donors (Supplementary Figure 3).

Taken together, the results of these experiments indicate that CG-EVs possess the ability to traverse the BBB, exhibit a specific affinity for glioblastoma, and importantly, demonstrate the potential to deliver Gd-DOTA to the glioblastoma site.

3.4. CG-EVs deliver cargo to glioblastoma in the brain

To further strengthen our findings, the next critical step involved assessing the ability of CG-EVs to facilitate the transportation of Gd-DOTA to a glioblastoma that had developed within the brain. This investigation was conducted within a model designed to maintain the integrity of the BBB. Instead of utilizing the conventional syngeneic orthotopic model, which requires an invasive intracranial injection of CT2A cells [16] directly into the brain parenchyma, we opted for a less invasive approach using intranasal delivery [17], a method that ensure the preservation of BBB integrity. In this technique, CT2A neurospheres were dissociated into a single-cell suspension of glioma stem cells (GSCs) at a concentration of 40,000 cells/μL. Eight droplets of 3 μL each containing GSCs were administered through the nostrils, resulting in the delivery of a total of 10E6 cells per animal. To establish this orthotopic glioblastoma model, we utilized immunocompetent transgenic NFκB-Luc2 mice. In this model, based on the C57BL/6 background (syngeneic with the CT2A cell line), the luciferase gene was placed under the control of an NFκB-responsive synthetic promoter [18], thus generating a reporter system specifically designed for studying inflammatory processes in animals using *in vivo* bioluminescence imaging. In our study, the NFκB-Luc2 reporter was employed to monitor the migration and growth of tumoral cells within the brain. Indeed, given the chronic inflammatory nature of the glioma microenvironment [19], we hypothesized that the overactivation of the NFκB pathway in animals subjected to intranasal administration of GSCs might be associated with

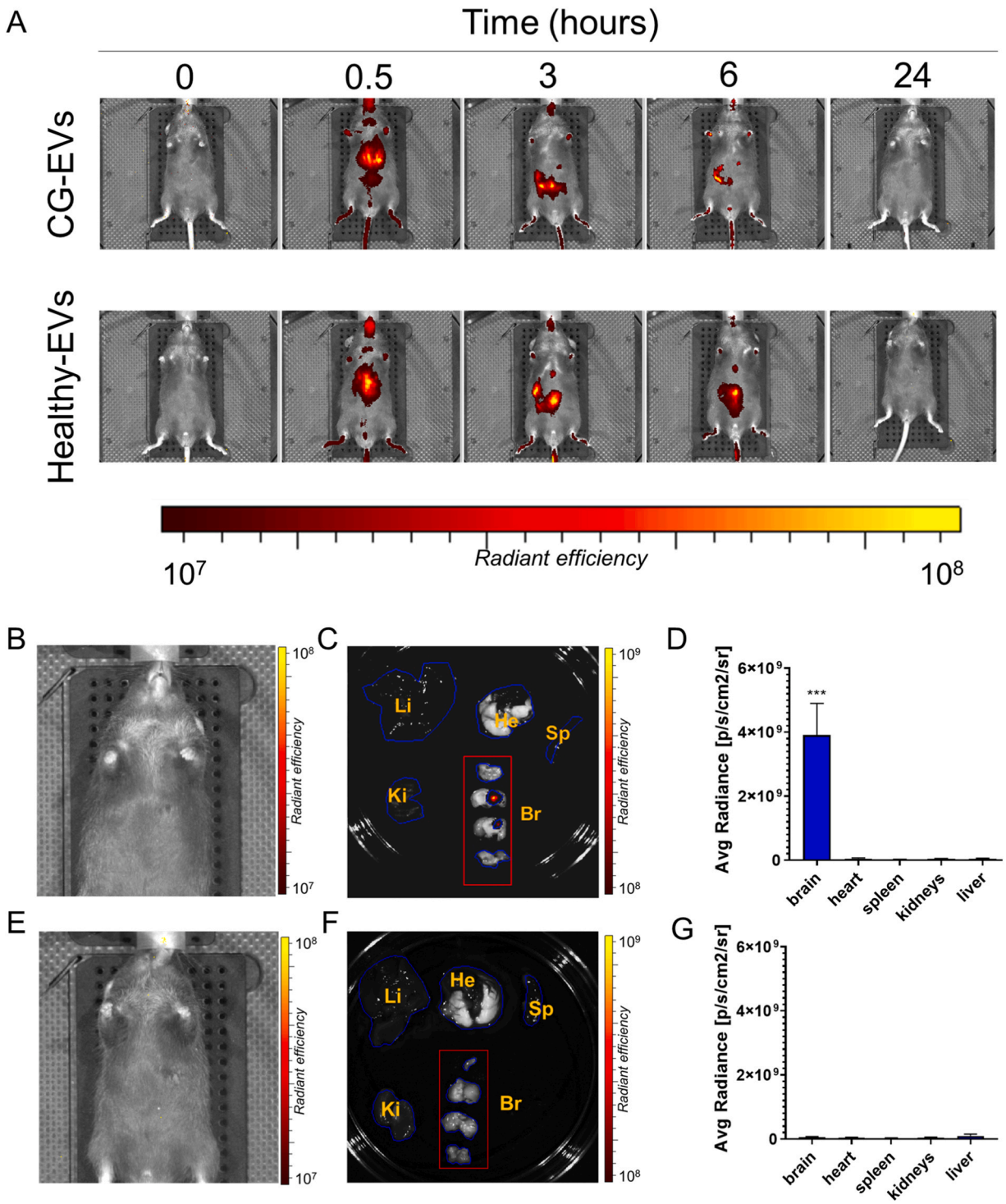

Fig. 2. Biodistribution of canine EVs in healthy mice. (A) Representative images of the comparative kinetics of distribution of ICG-loaded CG-EVs (upper row) and EVs isolated from healthy donors (Healthy-EVs, lower row). The fluorescence released by ICG (ex: 745 nm, em:840 nm) was *in vivo* acquired with an IVIS SpectrumCT imaging system and measured at 4 time points: before i.v. injection of the EVs (0 h), and at 0.5 h, 3 h, and 6 h after the i.v. injection of the EVs. The intensity of the fluorescence signal is represented with pseudocolors: yellow: high photon emission, bright red: medium photon emission, and dark red: low photon emission. (B) *in vivo* and (C) *ex vivo* imaging of a representative mouse i.v. injected with ICG-loaded CG-EVs and acquired at 24 h after the i.v. injection. Li: liver, He: heart and lungs, Sp: spleen, Ki: kidneys, Br: brain (here sliced in 4 macroareas, with the most rostral on top and the most caudal on the lower part of the image). The intensity of the fluorescence signal is represented with pseudocolors: yellow: high photon emission, bright red: medium photon emission, and dark red: low photon emission.) Quantification of the fluorescent signal released by the organs represented in C. Bars represent mean and S.E. of the average radiance measured in N = 3 mice. * ** : $p < 0.001$, t = 6.758, df= 4, eta squared: 0.9195, vs. liver. (E) *in vivo* and (F) *ex vivo* imaging of a representative mouse i.v. injected with ICG-loaded EVs from healthy donors and acquired at 24 h after the i.v. injection. Li: liver, He: heart and lungs, Sp: spleen, Ki: kidneys, Br: brain (here sliced in 4 macroareas, with the most rostral on top and the most caudal on the lower part of the image). The intensity of the fluorescence signal is represented with pseudocolors: yellow: high photon emission, bright red: medium photon emission, and dark red: low photon emission. D) Quantification of the fluorescent signal released by the organs represented in F. Bars represent mean and S.E. of the average radiance measured in N = 3 mice ($p = 0.17$, t = 1.060, df=4, eta squared: 0.2192, vs. liver).

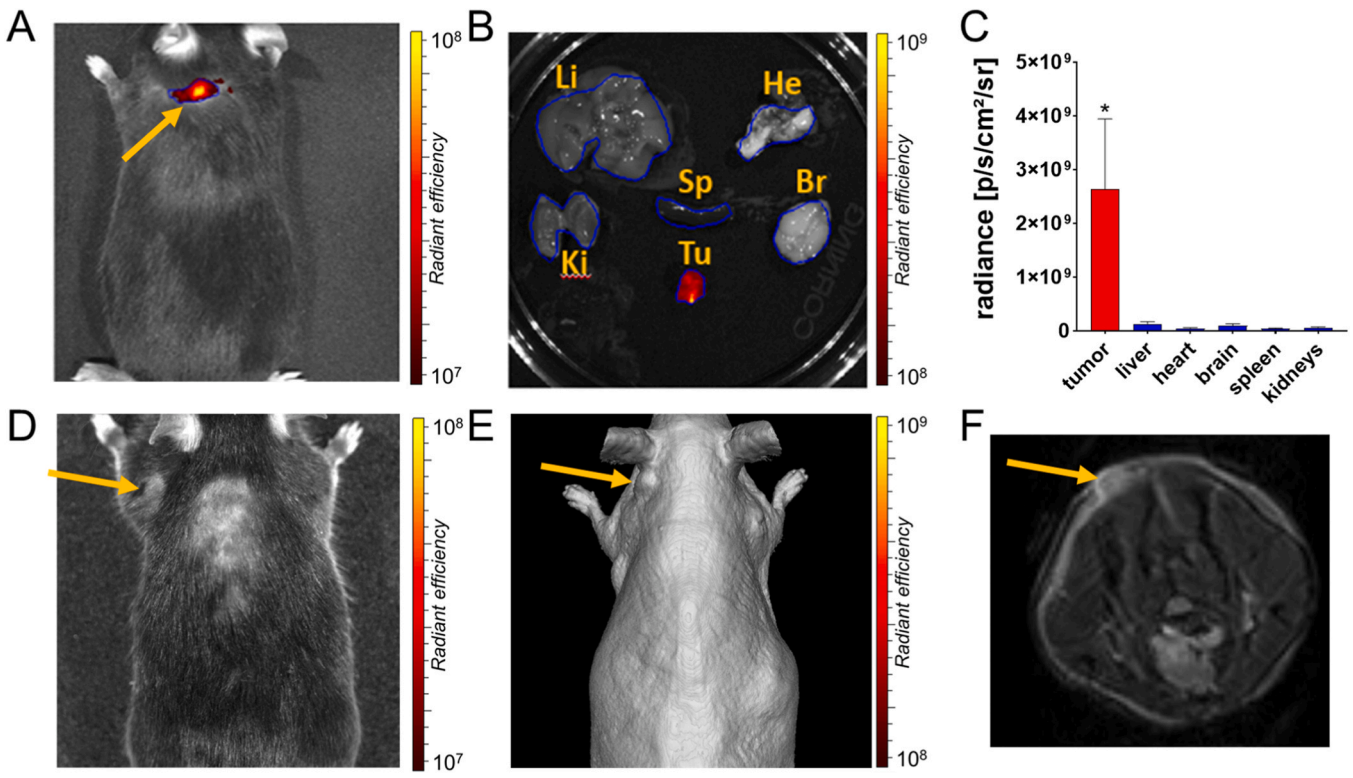

Fig. 3. Biodistribution of CG-EVs in a subcutaneous model of glioblastoma. (A) *in vivo* and (B) *ex vivo* imaging of a representative subcutaneous glioblastoma model i. v. injected with ICG-loaded CG-EVs and acquired at 24 h after the i.v. injection. Li: liver, He: heart and lungs, Sp: spleen, Ki: kidneys, Br: brain. The intensity of the fluorescence signal is represented with pseudocolors: yellow: high photon emission, bright red: medium photon emission, and dark red: low photon emission.C) Quantification of the fluorescent signal released by the organs represented in Fig. 2B. Bars represent mean and S.E. of the average radiance measured in N = 3 mice. * :$p < 0.05$, t = 1982, df= 4, eta squared: 0.4955, vs. liver. (D) Photograph and (E) three-dimensional CT scan reconstruction of a representative subcutaneous glioblastoma model i.v. injected with Gd-DOTA-loaded CG-EVs and acquired with MRI scans at 24 h after the i.v. injection. (F) Diffusion-weighted imaging (DWI) of the animal depicted in D and E acquired 24 h after the i.v. injection with Gd-DOTA-loaded CG-EVs. Yellow arrows indicate the position of the subcutaneous tumor.

tumor growth. The activation of the NFκB pathway in the cranial region was examined through bioluminescence imaging using an IVIS SpectrumCT imaging system in a series of weekly intervals involving three animals. During the initial week following intranasal inoculation of GSCs, the reporter's signal in the cranial region remained undetectable. However, starting from the second week post-inoculation (p.i.), a distinct signal began to emerge above the frontal and parietal bones, gradually intensifying over time (Fig. 4A). By the fifth week, the bioluminescence signal had become sufficiently robust (Fig. 4B) to allow a comprehensive 3D localization. This localization was achieved through the optical tomography capabilities of the IVIS SpectrumCT system, revealing the source of the bioluminescence in the subventricular zone (Fig. 4C).

This specific brain region, accessible via intranasal administration [20], is congruent with the initial stages of glioblastoma (GBM) development [21]. To validate these findings, the animals underwent the Evans Blue protocol, a widely recognized method for assessing BBB integrity [22], and then were humanely euthanized, and their brains were excised, fixed, and subsequently subjected to histological examinations to corroborate the presence of the tumor. Prior to the fixation process, fluorescence imaging (excitation: 620 nm, emission: 680 nm) was performed on the brains to assess the presence of Evans Blue within the brain tissue. This imaging step helped elucidating that the Evans Blue dye had not successfully permeated the brain parenchyma, thereby confirming the maintenance of BBB integrity (Supplementary Figure 4). Brain sections stained with haematoxylin and eosin further confirmed of the presence of highly proliferating neoplastic cells consistent with glioblastoma, infiltrating the subventricular zone. This finding documented that the inoculated glioma stem cells successfully migrated into the brain and began to infiltrate the central nervous system in the area highlighted by the 3D localization of the NFκB reporter signal (Fig. 4D). These findings clearly indicate the feasibility of creating an early-stage murine model of glioblastoma while preserving the integrity of the BBB, achieved through the intranasal administration of glioma stem cells. Subsequently, we employed this model to assess the capability of CG-EVs to precisely target GBM across the intact BBB. For this purpose, we intranasally inoculated 8 NFκB-Luc2 mice with 10E6 GSCs. After a 5-week period, these mice were intravenously administered through retro-orbital injection either CG-EVs (N = 4) or EVs sourced from healthy donors (N = 4), both loaded with Gd-DOTA. Following a 24-hour interval, MRI analysis was conducted to evaluate the accumulation of the contrast agent within the brain. MRI imaging distinctly revealed a hyperintense signal (Figs. 4E, F) localized in the subventricular zone, emanating from the accumulated contrast agent transported by CG-EVs. Once again, this signal was notably absent in the group that received EVs from healthy donors (Supplementary Figure 5A). Histological analysis of the brains from the animals that underwent MRI confirmed the presence of neoplastic cells consistent with glioblastoma across all subjects. Notably, the neoplastic cells were particularly evident in the region highlighted by the contrast agent in the CG-EV-treated group (Supplementary Figure 5B). Again, the maintenance of BBB integrity was confirmed by the Evans Blue assay, thereby corroborating the capability of CG-EV to cross the BBB. All in all, these results represent a proof-of concept that EVs isolated from glioma patients can be loaded with contrast agents, and possibly with other drugs with diagnostic or therapeutic activity, to transport the incapsulated molecule across the BBB to target tumors localized in the brain.

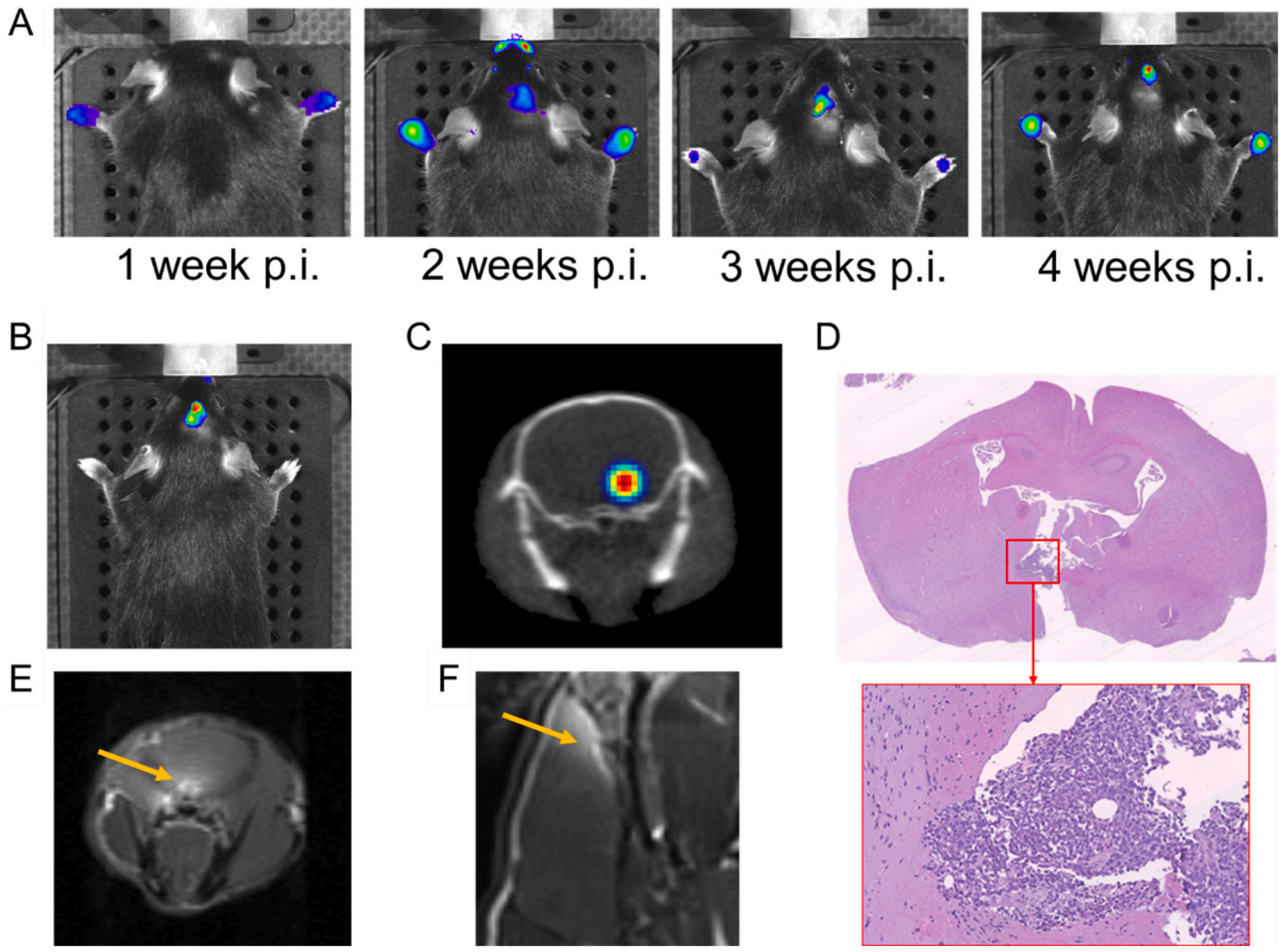

Fig. 4. Evaluation of the homing of CG-EV in an intranasal model of GBM. (A) Bioluminescence-based optical imaging of NFkB-Luc2 reporter activity in a representative mouse intranasally inoculated with GSCs. The pictures were acquired in the same mouse, in a series of weekly intervals starting from 1-week post inoculation (p.i.). The intensity of the bioluminescent signal, directly correlated with NFkB activity, is represented with pseudocolors: blue: low, yellow: medium, and red: high photon emission. (B) Bioluminescence-based optical imaging of NFkB-Luc2 reporter activity 5 weeks after the intranasal inoculation with GSCs. (C) The three-dimensional localization of the fluorescent signal was obtained by superimposing bioluminescent optical tomography data with CT scans. The intensity of the bioluminescent signal, directly correlated with NFkB activity, is represented with pseudocolors: blue: low, yellow: medium, and red: high photon emission. (D) Microscopical aspects of the subventricular zone in the brain excised from a mouse intranasally inoculated with GSCs, 5 weeks post inoculation. Hematoxylin and eosin (H&E) staining shows small cells with hyperchromatic nuclei and scant cytoplasm, with high mitotic rate and foci of necrosis, infiltrating the cerebral parenchyma (on the left) as evidenced in the magnified view. (E) Diffusion-weighted imaging (DWI) of the animal depicted in B and C acquired 24 h after the i.v. injection with Gd-DOTA-loaded CG-EVs. Yellow arrows indicate the hyperintense areas generated by the Gd-DOTA-loaded CG-EVs accumulating in the subventricular zone, where the GBM is located, as confirmed by histology (D and Supplementary Figure 4B).

4. Discussion

In this study, we conducted a comprehensive investigation into the potential of canine EVs as carriers for targeted glioblastoma imaging, highlighting their ability to deliver their cargo into the neoplastic tissue located inside the brain. This behavior aligns with our previous studies [9–11], which established that at extended time points (around 24 h) following intravenous injection, about half of the EVs originating from peripheral tumors accumulate at the tumor site (if present) due to spontaneous tropism. This affinity of cancer EVs for the tumoral tissue is independent of its location as the accumulation was observed also in a genetic model of cancer where the tumor arises within an organ [9]. In the absence of a tumor in the animal model, no accumulation is detected 24 h post intravenous administration of EVs originating from peripheral tumors, as they are either metabolized or excreted [11]. However, in this study, an unexpected distribution pattern was observed in EVs originating from tumors of the CNS (isolated from dogs with glioma), showing accumulation in the brain even in healthy mice without tumors. This unique observation suggested that EVs derived from dogs with glioma are capable of crossing the BBB and accumulating within the brain parenchyma, even under physiological conditions. We demonstrated the affinity of CG-EVs for glioblastoma tissue, emphasizing the specificity of CG-EVs for glioma compared to the control group treated with EVs from healthy donors. In particular, to assess the potential of CG-EVs in a clinically relevant context, we developed a minimally invasive model of early-stage GBM allowing for BBB integrity preservation while initiating glioma growth within the brain. Following the i.v. administration of CG-EVs loaded with Gd-DOTA, a gadolinium-based contrast agent, we detected hyperintense signals at the tumor site within the subventricular zone. All in all, this study shows the potential of utilizing CG-EVs as a potent tool for targeted drug delivery to intracranial tumors, even in the presence of an intact BBB.

These results build upon significant findings in the field of targeted drug delivery for cancer therapy, which has recently seen increased interest in harnessing the potential of EVs for theranostic purposes [23,24]. In this context, our research group previously made a noteworthy discovery: both human patients and dogs with glioma exhibit EVs in their plasma with a strong affinity for cancerous tissues, a feature absent

in healthy counterparts [11]. This finding suggested that tumors actively release EVs into the bloodstream, which tend to accumulate in their originating tumor sites.

The data presented in this manuscript add a new and important piece to this puzzle, demonstrating that EVs originating from brain cancer possess the inherent capacity to traverse the BBB. Indeed, they can leave the brain tumor and reach the bloodstream, allowing their isolation from the plasma of subjects affected by glioma, but – more surprisingly – they tend to return to the brain also in the absence of the originating tumor. This is one of the striking and unexpected results that we obtained in this study, since it suggests the existence of a chemotactic message released by resident brain cells, or the involvement of an active transport system through the BBB, as proposed by previous reports [13]. In the presence of a brain tumor, glioma-derived EVs show a tropism for the neoplastic cells as shown for various EVs of tumor origins [11,23,24], leading to an accumulation of their cargo in the tumoral area. Our current hypothesis is that EVs are released by neoplastic cells into the bloodstream, potentially promoting invasion and preparing metastatic niches in distant organs [25]. Additionally, they may return to their original tumors to promote growth [26] and evade the immune system [27]. While these hypotheses are of great biological interest, they fall outside the scope of our current work, which aims to provide evidence of the potential use of EVs derived from glioblastoma patients as delivery tools for anticancer therapy in glioblastoma.

Another important aspect of our study was modeling early-stage glioma, which our methodology effectively highlights. To this aim, we utilized a mouse model of glioblastoma that preserved the integrity of the BBB through intranasal cell inoculation, a method that we have previously demonstrated to efficiently deliver cells into the brain parenchyma [17]. This technique facilitated cell migration from the nasal cavity to the brain, likely through the olfactory and trigeminal nerve pathways at the upper nasal cavity, as the olfactory neuroepithelium is the only part of the central nervous system directly exposed to the external environment (see [17] and Supplementary Figure 6). The MRI imaging time frame was selected based on previously reported murine glioma models, typically requiring 3 to 8 weeks for tumor development in CT2A orthotopic models [28,29]. Given that CT2A gliomas elicit immune responses [16], we used NFkB-Luc reporter animals to monitor NFkB pathway activation, identifying the optimal 5-week post-inoculation interval, allowing detectable tumor growth while maintaining BBB integrity, as confirmed by Evans Blue experiments. Using Gd-DOTA, a contrast agent incapable of crossing the BBB in its standard form [30], we observed a contrast in the subventricular zone in MRI scans following the intravenous retro-orbital injection of Gd-DOTA-loaded CG-EVs. This, along with histological confirmation of tumoral cells, indicates the potential of patient-derived EVs to highlight gliomas in the initial stages and in the presence of an intact BBB.

The choice of studying dogs with glioma may initially appear as a limitation, however, it is a significant step toward conducting clinical studies on human subjects because canine brain malignancies exhibit remarkable similarities to their human counterparts in various aspects, including incidence rates, clinical manifestations, histopathological characteristics, and even survival durations [31]. Our driving hypothesis, guiding our exploration of canine EVs as a model to advance the pharmacological use of patient-derived EVs in humans, is based on our prior experience [11]. Indeed, our previous research revealed that canine EVs share the same tumor homing capabilities observed in human patient-derived EVs, which are able to accumulate - together with their cargo - into the tumoral tissue, independently from the tumor type or even the species bearing the tumor [9]. The body of evidence collected in the past years therefore, strongly suggest that the application in veterinary clinics of autologous EVs to target the tumors in large canine breeds could serve as a step forward towards the use of these nanoparticles for personalized medicine in humans.

The application of patient-derived EVs could be particularly relevant for glioblastoma patients, given the challenges involved in their management, often requiring complex and potentially uncomfortable treatment regimens. For example, using autologous patient-derived EVs for the delivery of diagnostics may overcome a major obstacle in GBM treatment: the absence of distinct initial symptoms for early diagnosis, which could greatly improve treatment outcomes. Therefore, our focus has been directed towards the application of CG-EVs for labeling glioblastoma with contrast agents, offering immediate solutions to address specific medical needs in this pathology. Clinical translation would be facilitated by the use of autologous EVs that are fully biocompatible with the donor and are expected to reduce the risk of immunogenicity compared to EVs of heterologous origin, or the risk of enhancing tumorigenesis associated with EVs derived from tumor cell lines [11,32]. The clinical application of this protocol could significantly enhance the sensitivity of other currently used diagnostic tools, potentially providing a detailed delineation of tumor margins and revealing normally undetectable metastases, thus addressing a major pitfall in oncological therapeutic planning — the uncertainty surrounding the local invasion's severity and the regional and distant extension of primary tumors [33]. Inaccurate surgical planning due to these uncertainties may result in incomplete or inadequate neoplastic excision. Precise margin detection pre- and intra-operatively is crucial for improving the surgeon's ability to eradicate diseases, especially for glioblastomas with complex phenotypes.

Moreover, the proof-of-concept provided by the current study not only demonstrates that CG-EVs can transport contrast agents into the brain for early brain tumor diagnosis but also opens avenues for utilizing therapeutic agents currently limited by their poor ability to cross the BBB. Agents like paclitaxel and doxorubicin, proven highly effective against gliomas *in vitro*, exhibit reduced efficacy within the central nervous system due to limited brain penetration [34,35]. This limitation stems from both poor brain permeability and rapid clearance from brain tissue via active transport [36]. Employing autologous patient-derived EVs as carriers offers several advantages, including the potential to transport drugs across the BBB and accumulate them within tumors, allowing precise release of chemotherapy agents directly to cancer cells. This targeted delivery approach not only allows for increased dosages of drugs that actively concentrate in glioma cells but also mitigates potential systemic toxicities and inflammatory reactions associated with chemotherapies [10]. This advantage creates a novel scenario for approved anti-neoplastic therapies, offering a local concentration that cannot be achieved through conventional systemic administration.

While our study focuses on practical applications rather than delving into the intricate mechanisms underlying tumor tropism, and does not elucidate the origins of these brain-targeting EVs, we are confident in the valuable insights presented within this manuscript. These findings signify a notable advancement in the clinical utilization of a potent resource - patient-derived EVs. This promising tool has the capacity to introduce novel strategies in the battle against cancer, even as certain aspects of its function and behavior warrant further investigation.

5. Conclusions

This study reports the promising potential of CG-EVs as effective carriers for targeted GBM imaging and drug delivery across the BBB. Our investigation has introduced novel insights into the biodistribution and tumor-targeting capabilities of these EVs in murine models. By highlighting their affinity for glioma tissue and their ability to traverse the BBB, we pave the way for innovative approaches in cancer theranostics, and provide a step forward in utilizing patient-derived EVs for precise diagnosis and treatment strategies. This work underscores the potential of EVs as a game-changing tool in the fight against glioblastoma and opens avenues for further exploration into their broader implications in cancer therapy.

Institutional review board statement

All animal experimentation was carried out in accordance with the Animal Research: Reporting of *In Vivo* Experiments (ARRIVE) guidelines and the European Guidelines for Animal Care. All animal experiments were approved by the Italian Ministry of Research and University, permission number: 214/2020. All the canine blood sampling for EVs isolation performed were approved by the Swiss Cantonal Animal Welfare Office, permission number: BE134/2020.

CRediT Author Statement

Alessandro Villa: Conceptualization, Formal analysis, Investigation, Methodology, Writing - original draft, Writing – review & editing. **Zemira De Mitri:** Conceptualization, Formal analysis, Investigation, Methodology, Writing—review & editing. **Simona Vincenti:** Conceptualization, Investigation, Methodology, Writing – review & editing. **Elisabetta Crippa:** Investigation. **Laura Castiglioni:** Methodology. **Paolo Gelosa:** Methodology. **Monica Rebecchi:** Methodology. **Delfina Tosi:** Methodology. **Electra Brunialti:** Investigation, Writing – review & editing. **Anna Oevermann:** Methodology. **Monica Falleni:** Methodology. **Luigi Sironi:** Writing – review & editing. **Lorenzo Bello:** Writing – review & editing. **Vincenzo Mazzaferro:** Writing – review & editing, Funding acquisition. **Paolo Ciana:** Conceptualization, Formal analysis, Methodology, Writing – original draft, Writing – review & editing, Funding acquisition.

Funding

The research leading to the results has received funding from AIRC under IG 2020 -ID.24914 project to P.C., and European Union — NextGenerationEU (PNRR M4C2-Investimento 1.4-CN00000041–23 PNRR_CN3RNA_SPOKE8 and PNRR_CN3RNA_SPOKE9) to P.C.

Declaration of Competing Interest

The authors declare that they have no known competing financial interests or personal relationships that could have appeared to influence the work reported in this paper.

Data availability

Data will be made available on request.

Appendix A. Supporting information

Supplementary data associated with this article can be found in the online version at doi:10.1016/j.biopha.2024.116201.

References

[1] S. Grochans, A.M. Cybulska, D. Siminska, J. Korbecki, K. Kojder, D. Chlubek, I. Baranowska-Bosiacka, Epidemiology of Glioblastoma Multiforme-Literature Review, Cancers 14 (10) (2022), https://doi.org/10.3390/cancers14102412.
[2] M. Ideguchi, K. Kajiwara, H. Goto, K. Sugimoto, S. Nomura, E. Ikeda, M. Suzuki, MRI findings and pathological features in early-stage glioblastoma, 289-97, J. Neurooncol 123 (2) (2015), https://doi.org/10.1007/s11060-015-1797-y.
[3] D. Zhuang, H. Zhang, G. Hu, B. Guo, Recent development of contrast agents for magnetic resonance and multimodal imaging of glioblastoma, J. Nanobiotechnol. 20 (1) (2022) 1–21.
[4] M.A. Subhan, S.S.K. Yalamarty, N. Filipczak, F. Parveen, V.P. Torchilin, Recent advances in tumor targeting via EPR effect for cancer treatment, J. Pers. Med. 11 (6) (2021) 571.
[5] N. Verburg, P.C. de Witt Hamer, State-of-the-art imaging for glioma surgery, Neurosurg. Rev. 44 (3) (2021) 1331–1343.
[6] O. Tyurikova, Y. Dembitskaya, K. Yashin, M. Mishchenko, M. Vedunova, I. Medyanik, V. Kazantsev, Perspectives in intraoperative diagnostics of human gliomas, Comput. Math. Methods Med. 2015 (2015) 479014, https://doi.org/10.1155/2015/479014.
[7] L.M. Doyle, M.Z. Wang, Overview of extracellular vesicles, their origin, composition, purpose, and methods for exosome isolation and analysis, Cells 8 (7) (2019), https://doi.org/10.3390/cells8070727.
[8] I.K. Herrmann, M.J.A. Wood, G. Fuhrmann, Extracellular vesicles as a next-generation drug delivery platform, Nat. Nanotechnol. 16 (7) (2021) 748–759.
[9] M. Garofalo, A. Villa, D. Crescenti, M. Marzagalli, L. Kuryk, P. Limonta, V. Mazzaferro, P. Ciana, Heterologous and cross-species tropism of cancer-derived extracellular vesicles, Theranostics 9 (19) (2019) 5681–5693, https://doi.org/10.7150/thno.34824.
[10] M. Garofalo, A. Villa, N. Rizzi, L. Kuryk, B. Rinner, V. Cerullo, M. Yliperttula, V. Mazzaferro, P. Ciana, Extracellular vesicles enhance the targeted delivery of immunogenic oncolytic adenovirus and paclitaxel in immunocompetent mice, J. Control Release 294 (2019) 165–175, https://doi.org/10.1016/j.jconrel.2018.12.022.
[11] A. Villa, M. Garofalo, D. Crescenti, N. Rizzi, E. Brunialti, A. Vingiani, P. Belotti, C. Sposito, S. Franze, F. Cilurzo, G. Pruneri, C. Recordati, C. Giudice, A. Giordano, M. Tortoreto, G. Beretta, D. Stefanello, G. Manenti, N. Zaffaroni, V. Mazzaferro, P. Ciana, Transplantation of autologous extracellular vesicles for cancer-specific targeting, Theranostics 11 (5) (2021) 2034–2047, https://doi.org/10.7150/thno.51344.
[12] L. Nieland, S. Mahjoum, E. Grandell, K. Breyne, X.O. Breakefield, Engineered EVs designed to target diseases of the CNS, J. Control. Release 356 (2023) 493–506.
[13] G. Morad, C.V. Carman, E.J. Hagedorn, J.R. Perlin, L.I. Zon, N. Mustafaoglu, T.-E. Park, D.E. Ingber, C.C. Daisy, M.A. Moses, Tumor-derived extracellular vesicles breach the intact blood–brain barrier via transcytosis, ACS nano 13 (12) (2019) 13853–13865.
[14] K.W. Witwer, D.C. Goberdhan, L. O'Driscoll, C. Thery, J.A. Welsh, C. Blenkiron, E. I. Buzas, D. Di Vizio, U. Erdbrugger, J.M. Falcon-Perez, Q.L. Fu, A.F. Hill, M. Lenassi, J. Lotvall, R. Nieuwland, T. Ochiya, S. Rome, S. Sahoo, L. Zheng, Updating MISEV: evolving the minimal requirements for studies of extracellular vesicles, J. Extra Vesicles 10 (14) (2021) e12182, https://doi.org/10.1002/jev2.12182.
[15] E. Binello, Z.A. Qadeer, H.P. Kothari, L. Emdad, I.M. Germano, Stemness of the CT-2A immunocompetent mouse brain tumor model: characterization in vitro, J. Cancer 3 (2012) 166.
[16] C.J. Liu, M. Schaettler, D.T. Blaha, J.A. Bowman-Kirigin, D.K. Kobayashi, A. J. Livingstone, D. Bender, C.A. Miller, D.M. Kranz, T.M. Johanns, Treatment of an aggressive orthotopic murine glioblastoma model with combination checkpoint blockade and a multivalent neoantigen vaccine, Neuro-Oncol. 22 (9) (2020) 1276–1288.
[17] A. Villa, P. Gelosa, L. Castiglioni, M. Cimino, N. Rizzi, G. Pepe, F. Lolli, E. Marcello, L. Sironi, E. Vegeto, Sex-specific features of microglia from adult mice, Cell Rep. 23 (12) (2018) 3501–3511.
[18] N. Rizzi, M. Rebecchi, G. Levandis, P. Ciana, A. Maggi, Identification of novel loci for the generation of reporter mice, Nucleic Acids Res. 45 (6) (2017) e37-e37.
[19] R. Al-Kharboosh, K. ReFaey, M. Lara-Velazquez, S.S. Grewal, J. Imitola, A. Quiñones-Hinojosa, Inflammatory mediators in glioma microenvironment play a dual role in gliomagenesis and mesenchymal stem cell homing: implication for cellular therapy, Mayo Clinic Proceedings: Innovations, Quality & Outcomes 4(4) (2020) 443–459.
[20] A. Mizutani, M. Kobayashi, M. Ohuchi, K. Sasaki, Y. Muranaka, Y. Torikai, S. Fukakusa, C. Suzuki, R. Nishii, S. Haruta, Indirect SPECT imaging evaluation for possible nose-to-brain drug delivery using a compound with poor blood–brain barrier permeability in mice, Pharmaceutics 14 (5) (2022) 1026.
[21] J. Kroonen, J. Nassen, Y.G. Boulanger, F. Provenzano, V. Capraro, V. Bours, D. Martin, M. Deprez, P. Robe, B. Rogister, Human glioblastoma-initiating cells invade specifically the subventricular zones and olfactory bulbs of mice after striatal injection, Int. J. Cancer 129 (3) (2011) 574–585.
[22] M.J. Wick, J.W. Harral, Z.L. Loomis, E.C. Dempsey, An optimized Evans blue protocol to assess vascular leak in the mouse, JoVE J. Vis. Exp. 139 (2018) e57037.
[23] N. Bie, T. Yong, Z. Wei, L. Gan, X. Yang, Extracellular vesicles for improved tumor accumulation and penetration, Adv. Drug Deliv. Rev. (2022) 114450.
[24] V.D. Nguyen, H.Y. Kim, Y.H. Choi, J.-O. Park, E. Choi, Tumor-derived extracellular vesicles for the active targeting and effective treatment of colorectal tumors in vivo, Drug Deliv. 29 (1) (2022) 2621–2631.
[25] A. Hoshino, B. Costa-Silva, T.-L. Shen, G. Rodrigues, A. Hashimoto, M. Tesic Mark, H. Molina, S. Kohsaka, A. Di Giannatale, S. Ceder, Tumour exosome integrins determine organotropic metastasis, Nature 527 (7578) (2015) 329–335.
[26] M.-Y. Kim, T. Oskarsson, S. Acharyya, D.X. Nguyen, X.H.-F. Zhang, L. Norton, J. Massagué, Tumor self-seeding by circulating cancer cells, Cell 139 (7) (2009) 1315–1326.
[27] A.S. Pathania, P. Prathipati, K.B. Challagundla, New insights into exosome mediated tumor-immune escape: clinical perspectives and therapeutic strategies, Biochim. Et. Biophys. Acta (BBA)-Rev. Cancer 1876 (2) (2021) 188624.
[28] V. Letchuman, L. Ampie, A.H. Shah, D.A. Brown, J.D. Heiss, P. Chittiboina, Syngeneic murine glioblastoma models: reactionary immune changes and immunotherapy intervention outcomes, Neurosurg. Focus 52 (2) (2022) E5.
[29] R. Martínez Murillo, A. Martínez, Standardization of an orthotopic mouse brain tumor model following transplantation of CT-2A astrocytoma cells, nº12, Histol. Histopathol. vol. 22 (2007) 2007.
[30] C. Leten, T. Struys, T. Dresselaers, U. Himmelreich, In vivo and ex vivo assessment of the blood brain barrier integrity in different glioblastoma animal models, J. Neuro-Oncol. 119 (2014) 297–306.
[31] J.W. Koehler, A.D. Miller, C.R. Miller, B. Porter, K. Aldape, J. Beck, D. Brat, I. Cornax, K. Corps, C. Frank, A revised diagnostic classification of canine glioma:

towards validation of the canine glioma patient as a naturally occurring preclinical model for human glioma, J. Neuropathol. Exp. Neurol. 77 (11) (2018) 1039–1054.
[32] K.W. Witwer, J. Wolfram, Extracellular vesicles versus synthetic nanoparticles for drug delivery, Nat. Rev. Mater. 6 (2) (2021) 103–106.
[33] A. Tieleman, K. Deblaere, D. Van Roost, O. Van Damme, E. Achten, Preoperative fMRI in tumour surgery, 2523-34, Eur. Radio. 19 (10) (2009), https://doi.org/10.1007/s00330-009-1429-z.
[34] D.Y. Zhang, C. Dmello, L. Chen, V.A. Arrieta, E. Gonzalez-Buendia, J.R. Kane, L. P. Magnusson, A. Baran, C.D. James, C. Horbinski, Ultrasound-mediated delivery of paclitaxel for glioma: a comparative study of distribution, toxicity, and efficacy of albumin-bound versus cremophor formulations, Clin. Cancer Res. 26 (2) (2020) 477–486.
[35] W.-H. Liao, M.-Y. Hsiao, Y. Kung, A.P.-H. Huang, W.-S. Chen, Investigation of the therapeutic effect of doxorubicin combined with focused shockwave on glioblastoma, Front. Oncol. 11 (2021) 711088.
[36] I. Sardi, O. Fantappiè, G. la Marca, M.G. Giovannini, A.L. Iorio, M. da Ros, S. Malvagia, S. Cardellicchio, L. Giunti, M. de Martino, Delivery of doxorubicin across the blood–brain barrier by ondansetron pretreatment: a study in vitro and in vivo, Cancer Lett. 353 (2) (2014) 242–247.